NeuroImage 329 (2026) 121841

Contents lists available at ScienceDirect

NeuroImage

journal homepage: www.elsevier.com/locate/ynimg

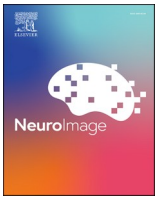

Associations between structural neuroimaging markers and neuropathology of Alzheimer's Disease

Stefan Frenzel [a,*], Stefan J. Teipel [b,c], Hans J. Grabe [a,c], for the National Alzheimer's Coordinating Center and the Alzheimer's Disease Neuroimaging Initiative[1]

[a] Department of Psychiatry and Psychotherapy, University Medicine Greifswald, 17475 Greifswald, Germany
[b] Department of Psychosomatic Medicine, University Medicine Rostock, 18147 Rostock, Germany
[c] German Center for Neurodegenerative Diseases (DZNE), Site Rostock/Greifswald, 17489 Greifswald, Germany

ARTICLE INFO

Keywords:
Alzheimer's disease
MRI
Autopsy
Neuropathology
Amyloid
Tau

ABSTRACT

Structural MRI is widely used for assessing the progression of Alzheimer's disease (AD). However, postmortem pathological examination remains the gold standard for confirming the diagnosis. We systematically investigated associations of structural MRI markers with AD neuropathology in well-characterized cohorts from Alzheimer's Disease Research Centres and the Alzheimer's Disease Neuroimaging Initiative. Data of 805 individuals who died between 2006 and 2024 were included. Markers of medial temporal lobe (MTL) and whole brain atrophy were determined from T1-weighted images acquired shortly before death. Two aggregate indices of AD-related brain atrophy (FSAD) and brain ageing (brainageR) were also included. Associations with neuropathology ratings were examined using ordinal logistic regression with proportional odds. At the time of MRI, median age was 78.5 years and 61 % had dementia. The median time between MRI and death was 4.6 years. At autopsy, 52 % had high Alzheimer's disease neuropathologic change (ADNC). In unadjusted analyses, ADNC most strongly correlated with volume of the MTL and the FSAD score (Spearman's ρ=-0.28 and 0.43). In adjusted analyses, the odds ratio associating low MTL volume with ADNC was 5.0 (95 % CI: 3.0-8.3); for a high FSAD score it was 11.0 (95 % CI: 6.6-18.0). MRI markers of AD generally were more strongly associated with tau than with amyloid beta pathology. AD neuropathology was associated with a distinct pattern of atrophy most pronounced in – but not restricted to – the MTL, differing from patterns seen in normal ageing. These results support the use of aggregate indices of AD-related atrophy over single-region morphometric characteristics for sample enrichment or as secondary outcomes in clinical trials.

1. Introduction

Alzheimer's disease (AD), the most common cause of dementia, is a progressive neurodegenerative disorder characterized by parenchymal deposits of amyloid beta (Aβ) plaques and neurofibrillary tangles (NFT) of tau protein (Braak and Braak, 1991, Thal et al., 2002, Hyman et al., 2012, Montine et al., 2012, Jack et al., 2018). While postmortem pathological examination remains the gold standard for confirming AD, structural MRI markers are widely used for assessing the progression of the disease (Frisoni et al., 2010, Leocadi et al., 2020). Especially for large-scale epidemiologic studies, automated MRI processing methods have become an invaluable alternative to visual assessments (Scheltens et al., 1992, Enkirch et al., 2018). In addition to volumetric markers derived from single regions (e.g. hippocampal volume), aggregate indices that combine atrophy information from multiple brain regions are increasingly being used (Cole et al., 2018, Franke and Gaser, 2019, Frenzel et al., 2020, Schwahn et al., 2022). While there is an extensive literature on the relationship between MRI markers and markers derived from other imaging modalities or biofluids (Jack and Holtzman, 2013, Pini et al., 2016, Haller et al., 2023), their relationship to the neuropathological changes the characterize AD are less well studied, particularly with respect to the current standard for assessing AD

* Corresponding author at: Department of Psychiatry and Psychotherapy, University Medicine Greifswald, 17475 Greifswald.
E-mail address: stefan.frenzel@uni-greifswald.de (S. Frenzel).

[1] Part of the data used in preparation of this article were obtained from the Alzheimer's Disease Neuroimaging Initiative (ADNI) database (adni.loni.usc.edu/). As such, the investigators within the ADNI contributed to the design and implementation of ADNI and/or provided data but did not participate in analysis or writing of this report. A complete listing of ADNI investigators can be found at: http://adni.loni.usc.edu/wp-content/uploads/how_to_apply/ADNI_Acknowledgement_List.pdf.

https://doi.org/10.1016/j.neuroimage.2026.121841
Received 7 October 2025; Received in revised form 3 March 2026; Accepted 3 March 2026
Available online 3 March 2026

neuropathology (Hyman et al., 2012, Montine et al., 2012, Dallaire-e-Théroux et al., 2017, Thaker et al., 2017, Denning et al., 2024).

Autopsy studies suggest that neuropathological lesions are ubiquitous in old age. While AD is most common, the majority of older individuals exhibit multiple types of neuropathologies (Boyle et al., 2018), which all contribute to cognitive decline and other clinical symptoms. At the same time, a substantial portion of cognitively normal individuals show signs of AD neuropathology (Bennett et al., 2006). MRI markers should therefore also be validated against the specific neuropathological changes in AD, not only against the clinical symptoms caused by it. This can help to develop MRI markers that are both sensitive and specific for AD pathology and complements efforts within the established AD biomarker validation framework (Frisoni et al., 2017), which ultimately requires effective treatments that are not yet available.

Volume of the medial temporal lobe (MTL) is among the best validated biomarkers of AD (Frisoni et al., 2017, Scheltens et al., 2021). There is substantial evidence from autopsy studies that AD neuropathology is associated with MTL atrophy, but also with volumetric changes in other brain structures on MRI (e.g. ventricular enlargement) (Dallaire-Théroux et al., 2017, Thaker et al., 2017, Denning et al., 2024). Although MRI-detectable atrophy typically reflects later stages of the disease process compared to molecular biomarkers (Jack et al., 2013), understanding their pathological correlates is essential for interpreting imaging findings, particularly in settings where MRI is the only available modality (e.g., in large-scale epidemiological studies). The aim of our study was therefore to investigate the strength of associations of commonly used structural markers derived from T1-weighted images with AD-related neuropathologic change (ADNC) (Hyman et al., 2012, Montine et al., 2012), using the latest autopsy data from Alzheimer's Disease Research Centres (ADRCs) and the Alzheimer's Disease Neuroimaging Initiative (ADNI). Total brain volume (supratentorial), ventricular volume, global cortical thickness, volume of white matter hypointensities, and volume of the MTL were included, as well as two previously published aggregate indices of brain ageing (Cole et al., 2018, Biondo et al., 2022) and AD-related brain atrophy (Frenzel et al., 2020) that both have not been associated with ADNC before. Associations with volumes of the primary structures of the MTL, i.e. hippocampus, entorhinal cortex, parahippocampal cortex, and the amygdala (Teipel et al., 2006), were also investigated.

AD neuropathology is often accompanied by additional brain pathologies. Inclusions of TAR DNA-binding protein 43 (TDP-43) within neurons of the MTL are particularly common in old age (Josephs et al., 2008, Josephs et al., 2014, Robinson et al., 2018). This has recently been formalized as a distinct disease entity termed limbic-predominant age-related TDP-43 encephalopathy neuropathologic change (LATE-NC) (Nelson et al., 2019, Wolk et al., 2025). LATE-NC is characterized by a hierarchical pattern of TDP-43 pathology originating in the amygdala and the hippocampus and later spreading to the cortex, and is independently associated with cognitive impairment and MTL atrophy (Katsumata et al., 2020, Josephs et al., 2017, Yu et al., 2020, Teipel and Grothe, 2023). Given its high prevalence in old age and the anatomical overlap with regions typically affected by AD, LATE-NC may substantially influence MRI measures commonly considered markers of AD. We therefore also investigated associations with LATE-NC in our study.

2. Materials and methods

2.1. Data sources

2.1.1. Alzheimer's Disease Research Centres

ADRCs are located at medical institutions across the United States and collectively follow thousands of research volunteers longitudinally. Data on participants demographics, medication, neuropsychological test results, clinical data, as well as neuropathology findings (if available) are collected and stored in a standardized way (Beekly et al., 2007, Besser et al., 2018). The National Alzheimer's Coordinating Center (NACC) was established in 1999 by the National Institute on Aging (NIA) and serves as the centralized data repository for the ADRCs (Beekly et al., 2004). MRI scans are not part of the standard protocol at all ADRCs. They are submitted to the NACC on a voluntary basis and are only available for a subset of participants.

All participants with data on AD neuropathology and at least one T1-weighted scan prior to death were included (see Supplementary Fig. 1). T1-weighted imaging was performed with varying protocols and scanning parameters. We included scans acquired at 1.5T and 3T with a spatial resolution (maximum voxel edge length) of a least 1.7mm. Scans with missing information on orientation as well as those with severe artefacts were excluded. If participants received brain MRI at multiple visits, only the last scan was considered. The NACC provides no information on potential overlap of cohorts from ADRCs with ADNI. Based on the date of birth and additional subject information, we identified five subjects who were enrolled in both studies. Only the last acquired MRI scan was taken into account. For this reason, three study participants were excluded. In total, data of 698 participants from 20 ADRCs who died between 2006 and 2024 were included in our study.

2.1.2. Alzheimer's Disease Neuroimaging Initiative

Data used in the preparation of this article were obtained from the ADNI database (adni.loni.usc.edu/). The ADNI was launched in 2003 as a public-private partnership, led by Principal Investigator Michael W. Weiner, MD. The primary goal of ADNI has been to test whether serial magnetic resonance imaging (MRI), positron emission tomography (PET), other biological markers, and clinical and neuropsychological assessment can be combined to measure the progression of mild cognitive impairment (MCI) and early Alzheimer's disease (AD) (Mueller et al., 2005, Weiner et al., 2017).

The ADNI includes subjects that are cognitively normal, subjects with MCI, as well as subjects with mild AD. The first study (ADNI-1) enrolled 800 participants (500 with MCI, 200 with early AD) from 56 study sites. Three-dimensional T1-weigthed MRI was performed at 1.5T by default. Since ADNI-2/GO, started in 2009, MRI was performed at 3T, except for participants that rolled over from ADNI-1. Scans from ADNI-1 and ADNI-GO/2 have undergone additional post-processing by the ADNI investigators including gradwarping, intensity correction, and have been scaled for gradient drift using phantom data. Scans from ADNI-3, started in 2016, did not undergo separate post-processing as scanners included vendor-specific processing routines for improving image quality. For more details regarding MRI in ADNI we refer to Jack et al. (2024) (Jack Jr et al., 2024). The neuropathology core of ADNI was established later in the course of ADNI (Perrin et al., 2024).

All participants with data on AD neuropathology and at least one T1-weighted scan prior to death were included (see Supplementary Fig. 1). Two subjects were excluded due to overlap with the ADRC cohorts. In total, 107 participants who died between 2007 and 2022 were included (latest available data as of May 2024). All of them received a T1-weighted brain MRI at least once during the baseline visit. If participants received brain MRI also at follow-up visits, only the last was considered.

2.2. Neuropathology data

Neuropathology data considered in this study were captured in the format of the Neuropathology Data Form of the NACC (Besser et al., 2018). In the majority of cases, data was collected with version 10 or 11 of the form, which includes information on Thal phase for Aβ plaques (Thal et al., 2002), Braak stage for neurofibrillary degeneration (Braak and Braak, 1991), and a semi-quantitative score for density of neocortical neuritic plaques proposed by the Consortium to Establish a Registry for Alzheimer's Disease (CERAD) (Montine et al., 2012, Mirra et al., 1993). These versions implement the latest guidelines for evaluating ADNC (Hyman et al., 2012, Montine et al., 2012). ADNC integrates

ratings of Thal phase for Aβ plaques (A score), NFTs (B score), and density of neuritic plaques (C score) into a single semi-quantitative score, which reflects the severity of AD-related neuropathology (ABC score; 0=Not AD, 1=Low, 2=Intermediate, 3=High) (Hyman et al., 2012, Montine et al., 2012). These four scores are the main outcomes of our study. An ABC score of 2 or 3 is considered sufficient explanation for dementia (Montine et al., 2012). Data of 133 participants at ADRCs were submitted in the older version 8 and 9 of the Neuropathology Data Form, which lack information on Thal phase and hence ADNC. These versions implement the older NIA-Reagan Institute diagnostic criteria (1995).

Data on presence of TDP-43 positive inclusions were available in a subset of 472 participants. LATE-NC stages were defined according to the criteria updated in 2019 adapted for NACC/ADNI data (Nelson et al., 2019, Woodworth et al., 2024). Presence of TDP-43 inclusions in the amygdala or the hippocampus, bot not both, were considered stage 1. Isolated presence in the entorhinal cortex (EC)/inferior temporal cortex (ITC) was also considered stage 1. Presence in both the amygdala and the hippocampus was considered stage 2. Additional presence in the neocortex was defined as stage 3. All other cases were considered as no LATE-NC (stage 0). Details on the definition of LATE-NC in the neuropathology data sets of ADNI and the NACC are provided in the Supplement.

2.3. Image processing

Cortical reconstruction and volumetric segmentation was performed with the Freesurfer image analysis suite (version 7.4.1), which is documented and freely available for download online (http://surfer.nmr.mgh.harvard.edu) (Fischl, 2012). The processing includes segmentation of cortical gray matter, white matter, subcortical nuclei, ventricles, estimation of total intracranial volume, and parcellation of the cerebral cortex into 34 regions per hemisphere (Desikan et al., 2006). In this study, overall brain volume (supratentorial), total ventricular volume (sum of lateral ventricles, third, and fourth ventricle), global cortical thickness (mean of left and right hemisphere), and volume of hypointensities in white matter were considered. The latter has been shown to correlate well with volume of hyperintensities on T2-weighted scans (Wei et al., 2019). MTL volume was defined as the sum of volumes of the hippocampus, amygdala, parahippocampal gyrus, and the entorhinal cortex. For some participants from ADRCs, multiple scans were acquired in a single session. Each of them was motion-corrected and averaged before the processing.

In addition, two previously published aggregate indices of AD-related brain atrophy and brain ageing were included. The FreeSurfer AD (FSAD) score was calculated as previously described in Frenzel et al. (2020) (Frenzel et al., 2020), except that the latest version of FreeSurfer (version 7.4.1) was used. Briefly, 169 morphometric characteristics were extracted from T1-weighted scans of participants with AD and cognitively normal ones from the ADNI-1 study (thicknesses of 68 cortical regions, and 101 volumes of subcortical brain regions). After standardizing them to mean zero and unit variance, a penalized logistic regression model was fitted. The FSAD score is defined as the linear predictor, i.e. it is equal to $\log(p/(1-p))$ with p denoting the estimated probability of having AD. A value of zero therefore means a 50 % risk of having AD. For values larger than zero, p is larger than 50 %. The following five characteristics have the greatest coefficients in the FSAD model (descending order): volume of left and right hippocampus, thickness of left entorhinal cortex, volume of left amygdala, and thickness of left rostral middle frontal cortex (see Fig. 4 in Frenzel et al. (Frenzel et al., 2020) for a spatially normalized three-dimensional visualization). Regression coefficients, as well mean values and standard deviations for standardizing the morphometric characteristics are listed in Supplementary Table 1.

For the calculation of brain age we relied on brainageR (v2.1), a free software for calculating brain-predicted age scores from raw T1-weighted MRI scans (https://github.com/james-cole/brainageR) (Cole et al., 2018, Biondo et al., 2022). The model was fitted to 3,377 healthy individuals from seven publicly-available datasets. BrainageR uses SPM12 (Statistical Parametric Mapping 12; https://www.fil.ion.ucl.ac.uk/spm/software/spm12) for pre-processing and normalisation. After additional data reduction, age is predicted from tissue concentration maps of gray matter, white matter, and cerebrospinal fluid using gaussian process regression. Quality was checked by visual inspection of the tissue density maps of each subject and was found to be sufficient in all cases.

The association between volumetric brain characteristics and AD neuropathology may be biased due to differences in image quality caused head movements during the scan (Reuter et al., 2015). To address this, we extracted several quality parameters from the output of FreeSurfer (fsqc v2.1.4; https://github.com/Deep-MI/fsqc (Esteban et al., 2017)). Ideally, surfaces generated by the cortical reconstruction have the topology of a closed surface but there may be defects due to segmentation errors. FreeSurfer implements automated methods for fixing these errors but a high initial number of those defects may indicate poor image quality. We considered the total number of defects before topology correction and the time it took to fix those errors. In addition, we calculated the signal-to-noise ratio of the segmented gray matter and white matter before and after intensity normalization, as well as the gray matter-white matter contrast signal-to-noise ratio across the cortex (mean of left and right hemisphere).

2.4. Statistical analyses

Neuropathology scores were modelled by ordinal logistic regressions with proportional odds (Walker-Duncan model) (Walker and Duncan, 1967, Harrell, 2015). Let Y denote such a rating with levels $0, 1, \ldots, k$ and higher values indicating a more severe neuropathology. For p independent variables and under the assumption of linearity, the exceedance probability, i.e. the probability of a rating of j or higher, is given by

$$P(Y \geq j|X) = \frac{1}{1 + \exp\left[-\left(\alpha_j + X^T\beta\right)\right]}$$

with $X^T\beta = \sum_{i=1}^{p} X_i\beta_i$, and $j \in 1, 2, \ldots, k$. Due to the inclusion of level-specific intercepts α_j, this model makes no assumption on the shape of the distribution of Y. For $k = 1$ one obtains the binary logistic regression model. The odds are given by $\exp\left(\alpha_j + X^T\beta\right)$, and the log odds for different cut-off values j differ only by the arithmetic difference of the corresponding intercepts. When increasing a single continuous independent variable X_m by one unit, while holding the other ones constant, the associated odds ratio (OR) is $\exp(\beta_m)$ and thus does not depend on the cut-off value j (proportional odds).

In this study, we used restricted cubic splines to model the relationships between continuous independent variables and neuropathology ratings in a flexible way without relying on the assumption of linearity. Three knots located at the 10 %, 50 %, and 90 % quantiles were used (Harrell, 2015). ORs were calculated by comparing the predicted odds at the 84 % quantile of exposure to the odds at the 16 % quantile from the complete sample, unless stated otherwise. This ensures comparability between MRI markers with different units or ranges of values. For a normally distributed variable, this corresponds to a comparison of mean plus/minus one standard deviation. The resulting ORs can directly be compared with those for binary variables with equal probabilities (Gelman, 2008). One advantage of the ordinal regression model is that it does not require selecting an arbitrary cut-off point. The resulting ORs can be interpreted as a summary measure of the association across all possible thresholds of the pathology scale. The overall goodness of fit was quantified by Nagelkerke's R^2, which generalizes the coefficient of determination of linear regression analysis to logistic regression models (ranging from 0 to 1) (Nagelkerke, 1991). We also calculated the concordance index C (Harrell, 2015), which is the

proportion of concordant pairs among all pairs of individuals. Concordance means that the individual with lower (or higher) estimated risk also has lower (or higher) rating of neuropathology. Values close to 0.5 indicate that the predictions are not much better than random guessing.

Ordinal regression models were fitted separately for each MRI marker and neuropathology score. Ideally, autopsies would be performed at the same time as the MRI, which is not feasible in practice. Median time between MRI and death was 4.6 years and reached values up to 16 years. For long time intervals, one expects correlation between MRI markers and neuropathology ratings to be weaker. To account for the time dependence, we included interactions with the MRI markers in the regression models, rather than excluding individuals with longer time intervals. ORs were then calculated for time intervals of 1 year (7 % quantile), 4.6 years (median), and 10 years (92 % quantile). Results are presented both unadjusted and additionally adjusted for age, sex, intracranial volume, study (ADRC, ADNI) (model 1). We also present results additionally adjusted for cognitive status (normal cognition, MCI, or dementia; model 2) as well as for LATE-NC.

Statistical analyses were conducted with *R* (version 4.4.2) and the *rms* package (version 7.0). Plots were generated with the package *ggplot2* (version 3.5.1) and *MRIcroGL* (Rorden, 2025).

3. Results

3.1. Sample characteristics

Data of 805 individuals who died between 2006 and 2024 were included (107 from ADNI and 698 from ADRCs). Sample characteristics are shown in Table 1. At the time of MRI, median age was 78.5 years and 43 % were females. Median time between MRI and death was 4.6 years and was as large as 16 years. Distributions within the studies and cognitive status are shown in Fig. 1. Participants from ADNI were slightly older, were more often male, and were less often cognitively normal than those from ADRCs. The vast majority either had dementia (61 %) or MCI (20 %). Scoring of ADNC according current NIA-AA guidelines was available for 656 participants. At autopsy, 52 % of them had high levels of ADNC (intermediate=18 %, low=17 %, none=13 %). Of those, 19 % did not have dementia. On the other hand, 24 % of participants with dementia did not have high ADNC at autopsy (see Fig. 1F). Data on LATE-NC was available in a subset of 472 individuals. LATE-NC was slightly more frequent in cases of high ADNC (42 %) compared to those with low ADNC (34 %) and no ADNC (22 %).

3.2. Associations of MRI markers with neuropathology ratings

3.2.1. Pairwise rank correlations

Pairwise rank correlations (Spearman's ρ) among all variables considered in this study are shown in Supplementary Fig. 2. Neuropathology ratings were highly correlated among each other, with correlation values ranging from 0.73 to 0.92. Correlation of ADNC with cognitive status (1=normal cognition, 2=MCI, 3=dementia) was 0.45. Correlations of ADNC with MRI markers ranged from -0.28 (MTL volume) to 0.43 (FSAD score). Correlations with AD neuropathology according the older NIA-Reagan Institute criteria (available in the subset of participants whose autopsies were reported with version 8 and 9 of the Neuropathology Data Form) ranged from -0.36 (MTL volume) to 0.41 (FSAD score). Both in subsamples of individuals from ADRCs and from ADNI, ADNC also most strongly correlated with MTL volume and the FSAD score (Supplementary Fig.s 3 and 4).The correlation between ADNC and LATE-NC was 0.07. LATE-NC was at least as strongly associated with ventricular volume and MTL volume as ADNC. Overall, values ranged from -0.31 (MTL volume) to 0.27 (FSAD score).

3.2.2. Ordinal logistic regression analyses

In analyses adjusted for differences in age, sex, intracranial volume, study, magnetic field strength, and time between MRI and death (model

Table 1
Sample characteristics.

	ADNI	ADRCs	Overall
Sample size	107	698	805
Age at time of MRI, years	80 (72.5, 86.9)	78 (64.9, 87.5)	78.5 (66.1, 87.5)
Females (%)	28 (26)	315 (45)	343 (43)
Years of Education	16 (13, 20)	16 (12, 18)	16 (12, 18)
Age at time of death, years	84.8 (77.5, 91.5)	83 (70, 92)	84 (70.6, 92)
Survival time, years	3.7 (1.6, 6.9)	4.7 (1.8, 8.3)	4.6 (1.8, 8.1)
Year of death			
2006 - 2010	12 (11)	49 (7)	61 (8)
2010 - 2015	41 (38)	184 (26)	225 (28)
2016 - 2020	49 (46)	308 (44)	357 (44)
2021 - 2024	5 (5)	157 (22)	162 (20)
Time between MRI and closest study visit, days	0 (-1, 9)	14 (-123, 91)	7 (-75, 85)
Cognitive status at closest study visit %)			
Normal cognition	10 (9)	141 (20)	151 (19)
Mild cognitive impairment	24 (22)	138 (20)	162 (20)
Dementia	73 (68)	419 (60)	492 (61)
Neuroimaging			
Magnetic field strength (%)			
1.5 T	62 (58)	390 (56)	452 (56)
3 T	45 (42)	308 (44)	353 (44)
Voxel edge length (maximum), mm	1.2 (1.2, 1.25)	1.2 (1, 1.5)	1.2 (1, 1.5)
Intracranial volume, ml	1545 (1407, 1733)	1519 (1352, 1711)	1527 (1361, 1714)
Supratentorial brain volume, ml	854 (767, 964)	864 (769, 974)	863 (768, 972)
Total ventricular volume, ml	63 (39, 93)	53 (34, 82)	54 (34, 83)
White matter hypointensities volume, ml	7.2 (3.2, 20.4)	5.2 (2.1, 14.5)	5.4 (2.2, 14.8)
Global cortical thickness, mm	2.16 (1.99, 2.29)	2.19 (2.04, 2.32)	2.19 (2.03, 2.31)
Medial temporal lobe volume, ml	14.1 (11.9, 16.9)	15.2 (12.6, 17.8)	15.1 (12.5, 17.7)
Brain age (brainageR), years	80 (74.7, 86.8)	77.9 (67, 85)	78.3 (67.9, 85.4)
FreeSurfer-based AD Score (FSAD)	3.1 (-1.1, 6.3)	1.1 (-2.6, 5)	1.3 (-2.5, 5.2)
Autopsy data			
Neuropathology data form version (%)			
8/9	0 (0)	133 (19)	133 (17)
10	83 (78)	382 (55)	465 (58)
11	24 (22)	183 (26)	207 (26)
Post-mortem interval, hours	9 (3, 22)	11 (5, 24)	11 (5, 24)
missing (%)	2 (2)	190 (27)	192 (24)
Thal phase (A score) (%)			
0	5 (5)	84 (12)	89 (11)
1	7 (7)	66 (9)	73 (9)
2	13 (12)	51 (7)	64 (8)
3	82 (77)	356 (51)	438 (54)
missing	0 (0)	141 (20)	141 (18)
Braak stage (B score) (%)			
0	1 (1)	50 (7)	51 (6)
1	21 (20)	131 (19)	152 (19)
2	14 (13)	159 (23)	173 (21)
3	71 (66)	358 (51)	429 (53)
missing	0 (0)	0 (0)	0 (0)
CERAD score for neuritic plaques (C score) (%)			
0	21 (20)	162 (23)	183 (23)
1	13 (12)	87 (12)	100 (12)
2	11 (10)	166 (24)	177 (22)
3	62 (58)	282 (40)	344 (43)
missing	0 (0)	1 (0)	1 (0)
AD neuropathologic change (ADNC, ABC score) (%)			
0	5 (5)	82 (12)	87 (11)
1	19 (18)	94 (13)	113 (14)
2	14 (13)	104 (15)	118 (15)
3	69 (64)	269 (39)	338 (42)
missing	0 (0)	149 (21)	149 (19)
LATE-NC (%)			
0	52 (49)	244 (35)	296 (37)
1	14 (13)	37 (5)	51 (6)

(*continued on next page*)

Table 1 (*continued*)

	ADNI	ADRCs	Overall
2	21 (20)	62 (9)	83 (10)
3	13 (12)	29 (4)	42 (5)
missing	7 (7)	326 (47)	333 (41)

Values are counts (percentage) for categorical variables and medians (16 %, 84 % quantile) for continuous variables. For some of the participants from ADRCs, autopsy results were captured in data form versions prior to version 10 (n=133). These older versions lack information on Thal phase for Aβ plaques and therefore also ADNC. Limbic-predominant age-related TDP-43 encephalopathy neuropathologic change (LATE-NC) was defined based on the presence of inclusions of TAR DNA-binding protein 43 (TDP-43) in the amygdala, hippocampus, entorhinal cortex/inferior temporal cortex, and neocortex (reported since version 10).

1), ADNC was most strongly associated with MTL volume and the FSAD score. As we included an interaction with time between MRI and death, the odds ratios depend on the length of this time interval. Table 2 shows results for the median value of 4.6 years. Compared to low values, high MTL volume was associated with an odds ratio of 0.20 (95 % CI: 0.12-0.33), and a high FSAD score associated with an odds ratio of 11.0 (95 % CI: 6.6-18.0). Models including either one of these two markers showed acceptable overall goodness of fit and discrimination (Nagelkerke's R^2 = 0.21 and 0.3; C = 0.71 and 0.75). For comparison, associations with high ADNC in binary logistic regression models are shown in Supplementary Table 2. Associations were slightly stronger but overall similar to those in ordinal logistic regression models. Again, MTL volume and the FSAD score most strongly associated with high ADNC. The estimated odds ratios associated with low MTL volume and high FSAD score were 6.7 and 18.1, respectively.

MTL volume and the FSAD score were more strongly associated with Braak stage (B score) than with Thal phase (A score) or density of neuritic plaques (C score). Associations of ADNC with markers reflecting global ageing-related brain changes, such as brain volume or brain age, were substantially weaker . The estimated probability of low and high ADNC, as well as mean ADNC for the five MRI markers most strongly associated with ADNC (largest Nagelkerke's R^2) are shown in Fig. 2C. MRI marker values were monotonously related to mean ADNC, i.e. more pronounced atrophy was always associated with higher ADNC. The overall slope was largest for the FSAD score, with a difference of 1.9 points when comparing the 2.5 % with the 97.5 % quantile (indicated by dotted lines).

When additionally taking into account differences in cognitive status, associations between MRI markers and ADNC were about half as strong (model 2). Results for subsamples of individuals who were scanned at 1.5T were largely similar to those scanned at 3T, as were results for participants from ADRCs compared to those of ADNI, with much larger confidence intervals due to the low sample size for the latter (results shown in Supplementary Fig. 6). Notably, association of MTL volume with ADNC and its subscores were substantially weaker in individuals with dementia compared to those without, suggesting sensitivity to the severity of AD neuropathology primarily in the early phase of AD. The odds ratios associated with high MTL volume were 0.57 (95 % CI 0.28-1.15) and 0.24 (95 % CI 0.12-0.48).

In the subsample with available data on LATE-NC, additional adjustment for LATE-NC did not substantially change the associations

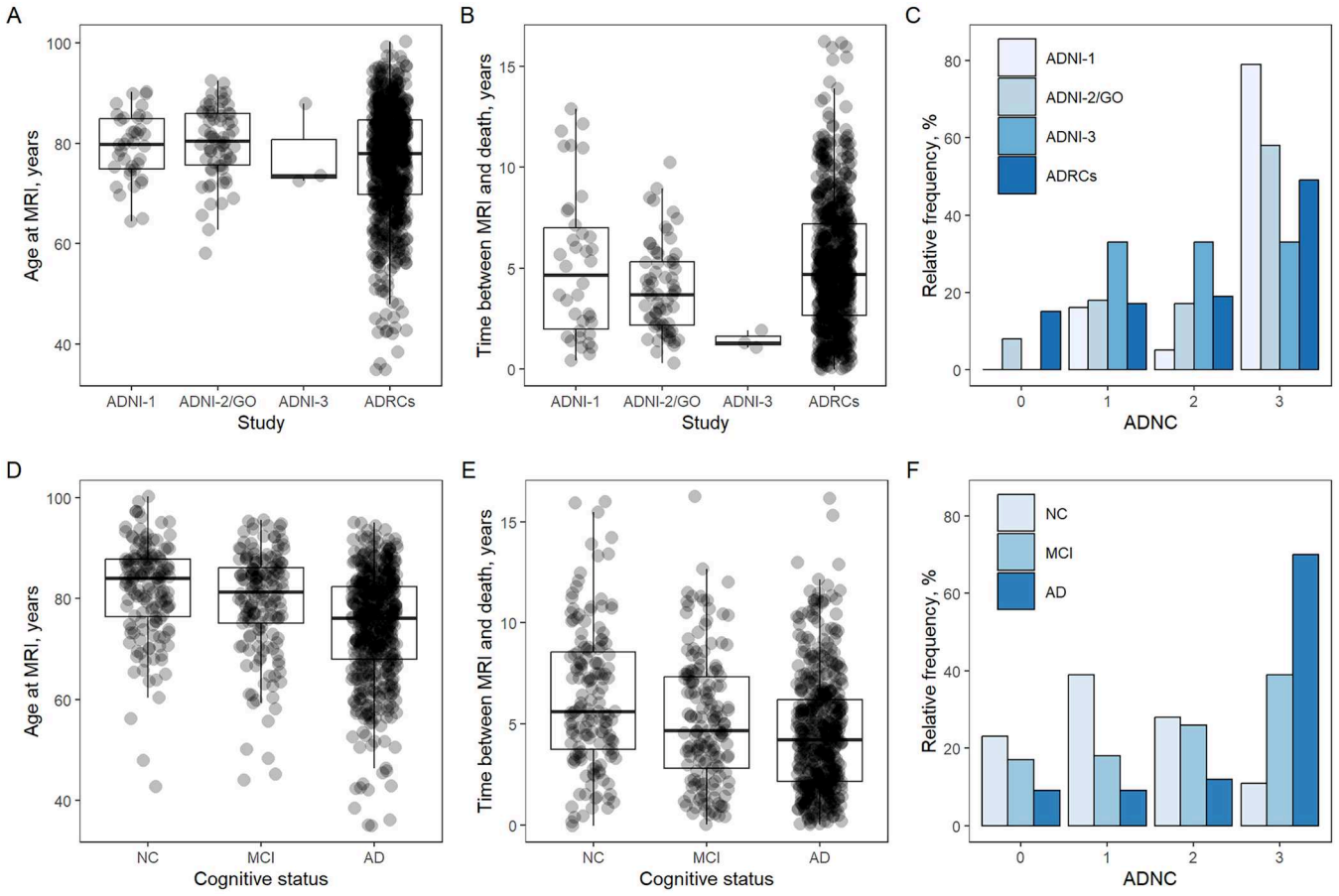

Fig. 1. Characteristics of participants from Alzheimer's Disease Research Centres and the Alzheimer's Disease Neuroimaging Initiative that were included in this study (n=805). Distribution of age at MRI, time between MRI and death, and AD neuropathologic change (ADNC) within the studies (A–C), as well as within the cognitive status at the neuropsychological evaluation closest to MRI (D–F).

Table 2
Associations of MRI markers with AD neuropathology and limbic-predominant age-related TDP-43 encephalopathy neuropathologic change.

		Unadjusted			Model 1			Model 2		
	n	R_N^2	*C*	OR (95 % CI)	R_N^2	*C*	OR (95 % CI)	R_N^2	*C*	OR (95 % CI)
Thal phase (A score)										
Intracranial volume	664	0	0.53	1.01 (0.65, 1.56)	0.07	0.61	1.09 (0.66, 1.80)	0.22	0.73	1.10 (0.64, 1.88)
Supratentorial brain volume	664	0.01	0.55	0.78 (0.50, 1.21)	0.08	0.62	0.53 (0.27, 1.04)	0.22	0.73	1.02 (0.50, 2.09)
Total ventricular volume	664	0.03	0.58	1.82 (1.15, 2.90)	0.09	0.64	2.23 (1.33, 3.76)	0.22	0.73	1.15 (0.66, 2.00)
WMH volume	664	0.03	0.57	1.79 (1.04, 3.06)	0.09	0.63	2.35 (1.28, 4.30)	0.22	0.73	1.59 (0.86, 2.95)
Global cortical thickness	664	0.06	0.6	0.37 (0.24, 0.57)	0.12	0.66	0.29 (0.18, 0.47)	0.24	0.74	0.47 (0.28, 0.77)
Medial temporal lobe volume	664	0.07	0.62	0.39 (0.25, 0.62)	0.12	0.67	0.33 (0.20, 0.55)	0.23	0.74	0.69 (0.40, 1.19)
Brain age (brainageR)	664	0.05	0.59	1.81 (1.14, 2.87)	0.1	0.65	2.17 (1.29, 3.65)	0.23	0.74	1.47 (0.85, 2.54)
FreeSurfer AD score (FSAD)	664	0.16	0.7	6.43 (3.94, 10.50)	0.21	0.72	7.06 (4.20, 11.86)	0.26	0.75	3.63 (2.09, 6.30)
Braak stage (B score)										
Intracranial volume	805	0.02	0.56	1.16 (0.80, 1.69)	0.09	0.61	1.28 (0.84, 1.94)	0.27	0.73	1.39 (0.89, 2.16)
Supratentorial brain volume	805	0.04	0.58	0.77 (0.52, 1.12)	0.12	0.63	0.43 (0.25, 0.75)	0.27	0.74	0.84 (0.47, 1.50)
Total ventricular volume	805	0.07	0.61	2.90 (1.91, 4.40)	0.15	0.66	3.89 (2.43, 6.23)	0.28	0.74	2.24 (1.37, 3.64)
WMH volume	805	0.04	0.57	1.86 (1.17, 2.97)	0.11	0.63	2.25 (1.33, 3.78)	0.27	0.74	1.60 (0.94, 2.74)
Global cortical thickness	805	0.09	0.63	0.32 (0.22, 0.46)	0.16	0.67	0.27 (0.18, 0.39)	0.29	0.75	0.40 (0.26, 0.59)
Medial temporal lobe volume	805	0.16	0.66	0.25 (0.17, 0.38)	0.22	0.7	0.19 (0.12, 0.29)	0.31	0.76	0.37 (0.23, 0.60)
Brain age (brainageR)	805	0.07	0.6	2.27 (1.52, 3.39)	0.12	0.64	2.40 (1.54, 3.74)	0.29	0.75	1.88 (1.18, 2.98)
FreeSurfer AD score (FSAD)	805	0.25	0.73	11.79 (7.39, 18.82)	0.3	0.75	12.99 (7.99, 21.14)	0.36	0.78	7.19 (4.33, 11.94)
CERAD score for neuritic plaques (C score)										
Intracranial volume	804	0.01	0.54	1.37 (0.96, 1.95)	0.1	0.63	1.57 (1.05, 2.35)	0.23	0.71	1.73 (1.14, 2.62)
Supratentorial brain volume	804	0.01	0.55	0.88 (0.61, 1.25)	0.12	0.65	0.38 (0.22, 0.65)	0.23	0.71	0.64 (0.37, 1.11)
Total ventricular volume	804	0.04	0.58	2.43 (1.63, 3.65)	0.13	0.66	3.05 (1.95, 4.77)	0.24	0.71	1.82 (1.14, 2.89)
WMH volume	804	0.02	0.56	1.45 (0.93, 2.26)	0.12	0.64	1.95 (1.19, 3.20)	0.24	0.71	1.45 (0.88, 2.41)
Global cortical thickness	804	0.05	0.59	0.42 (0.30, 0.60)	0.14	0.66	0.36 (0.25, 0.52)	0.24	0.72	0.52 (0.36, 0.76)
Medial temporal lobe volume	804	0.09	0.62	0.41 (0.28, 0.59)	0.18	0.69	0.30 (0.20, 0.45)	0.26	0.73	0.54 (0.35, 0.83)
Brain age (brainageR)	804	0.04	0.57	1.79 (1.22, 2.62)	0.12	0.65	2.31 (1.51, 3.55)	0.24	0.72	1.74 (1.12, 2.70)
FreeSurfer AD score (FSAD)	804	0.18	0.68	6.54 (4.34, 9.84)	0.24	0.71	6.34 (4.16, 9.67)	0.29	0.74	3.73 (2.39, 5.81)
AD neuropathologic change (ABC score)										
Intracranial volume	656	0.01	0.54	1.11 (0.74, 1.66)	0.09	0.63	1.09 (0.69, 1.74)	0.28	0.74	1.08 (0.66, 1.76)
Supratentorial brain volume	656	0.02	0.56	0.77 (0.51, 1.17)	0.12	0.65	0.41 (0.22, 0.76)	0.28	0.75	0.80 (0.42, 1.54)
Total ventricular volume	656	0.04	0.59	2.23 (1.44, 3.45)	0.14	0.66	3.12 (1.90, 5.13)	0.29	0.75	1.60 (0.95, 2.69)
WMH volume	656	0.02	0.56	1.44 (0.88, 2.36)	0.11	0.64	2.21 (1.27, 3.85)	0.28	0.74	1.49 (0.84, 2.63)
Global cortical thickness	656	0.07	0.61	0.35 (0.23, 0.52)	0.16	0.67	0.26 (0.17, 0.40)	0.3	0.75	0.41 (0.26, 0.65)
Medial temporal lobe volume	656	0.12	0.64	0.30 (0.20, 0.46)	0.21	0.71	0.20 (0.12, 0.33)	0.32	0.76	0.41 (0.25, 0.69)
Brain age (brainageR)	656	0.05	0.58	1.92 (1.24, 2.98)	0.13	0.67	2.78 (1.69, 4.59)	0.3	0.76	1.88 (1.11, 3.17)
FreeSurfer AD score (FSAD)	656	0.24	0.72	10.24 (6.34, 16.54)	0.3	0.75	10.94 (6.64, 18.01)	0.36	0.78	5.82 (3.45, 9.82)
Limbic-predominant age-related TDP-43 encephalopathy (LATE-NC)										
Intracranial volume	472	0.1	0.64	1.02 (0.58, 1.82)	0.15	0.68	1.19 (0.61, 2.31)	0.23	0.73	1.27 (0.64, 2.49)
Supratentorial brain volume	472	0.07	0.63	0.62 (0.35, 1.10)	0.16	0.7	0.23 (0.10, 0.53)	0.24	0.74	0.40 (0.17, 0.93)
Total ventricular volume	472	0.12	0.66	2.28 (1.20, 4.34)	0.17	0.69	1.51 (0.75, 3.02)	0.24	0.73	1.03 (0.50, 2.12)
WMH volume	472	0.13	0.65	3.11 (1.63, 5.93)	0.18	0.7	1.89 (0.92, 3.89)	0.26	0.74	1.40 (0.66, 2.99)
Global cortical thickness	472	0.09	0.64	0.58 (0.35, 0.96)	0.16	0.69	0.58 (0.34, 1.00)	0.23	0.73	0.80 (0.46, 1.42)
Medial temporal lobe volume	472	0.17	0.69	0.31 (0.17, 0.57)	0.27	0.75	0.18 (0.09, 0.36)	0.29	0.76	0.24 (0.12, 0.49)
Brain age (brainageR)	472	0.11	0.65	2.75 (1.54, 4.90)	0.15	0.68	1.92 (1.00, 3.68)	0.22	0.73	1.47 (0.76, 2.84)
FreeSurfer AD score (FSAD)	472	0.18	0.7	3.91 (2.01, 7.61)	0.25	0.74	4.17 (2.06, 8.43)	0.28	0.76	2.99 (1.43, 6.26)

Model 1 = adjusted for age, sex, intracranial volume, study, magnetic field strength, and time between MRI and death (4.6 years).
Model 2 = model 1 + cognitive status (normal cognition, mild cognitive impairment, or dementia).
R_N^2 – Nagelkerke's R^2, *C* – concordance index, OR – odds ratio, CI – confidence interval.

between MRI markers and AD neuropathology ratings (Supplementary Table 5). However, several MRI markers showed strong associations with LATE-NC (Fig. 2B). Both low total brain volume and low MTL volume were associated with greater odds of LATE-NC than ADNC at autopsy. MTL volume exhibited the strongest association, with lower volume being associated with 5.6-fold higher odds of LATE-NC and 2.6-fold higher odds of ADNC under model 1. High FSAD scores were associated with 4.5-fold higher odds of LATE-NC and 8-fold higher odds of ADNC in this subsample.

3.2.3. *Influence of the time interval between mri and death*

Associations of MRI markers with neuropathology were weaker for large time intervals between MRI and death (see Fig. 2A). One year after MRI, the odds ratio associating high MTL volume with ADNC was 0.11 (95 % CI: 0.05-0.27) and ten years after MRI it was 0.57 (95 % CI: 0.31-1.06). Ten years after MRI, the only MRI markers that were associated with odds ratios statistically significantly different from one (at the 5 % level) were global cortical thickness (OR=0.43, 95 % CI: 0.26-0.71) and the FSAD score (OR=2.5, 95 % CI: 1.5-4.3). However, confidence intervals for brain volume and MTL volume largely overlapped with that of global cortical thickness. These differences in statistical significance are therefore not statistically significant themselves.

3.2.4. *The role of image quality parameters*

Image quality characteristics are shown in Supplementary Table 3. High image quality was associated with decreased odds of AD-related neuropathology. For ADNC, the odds ratio associated with high gray matter signal-to-noise ratio in original images was 0.37 (95 % CI: 0.23-0.58) and was slightly weaker after intensity normalization (OR=0.45, 95 % CI: 0.30-0.72) (model 1; Supplementary Fig. 5). Odds ratios associated with high white matter signal-to-noise ratio were 0.53 (95 % CI: 0.33-0.85) for the original images and 0.81 (95 % CI: 0.53-1.24) after intensity normalization. When additionally adjusting for all image quality parameters, the estimated odds ratios associated with MRI markers did not change much and remained within the confidence intervals obtained under model 1. Thus, the associations of MRI markers with Alzheimer's disease neuropathology observed in our study could not be explained by differences in the considered image quality

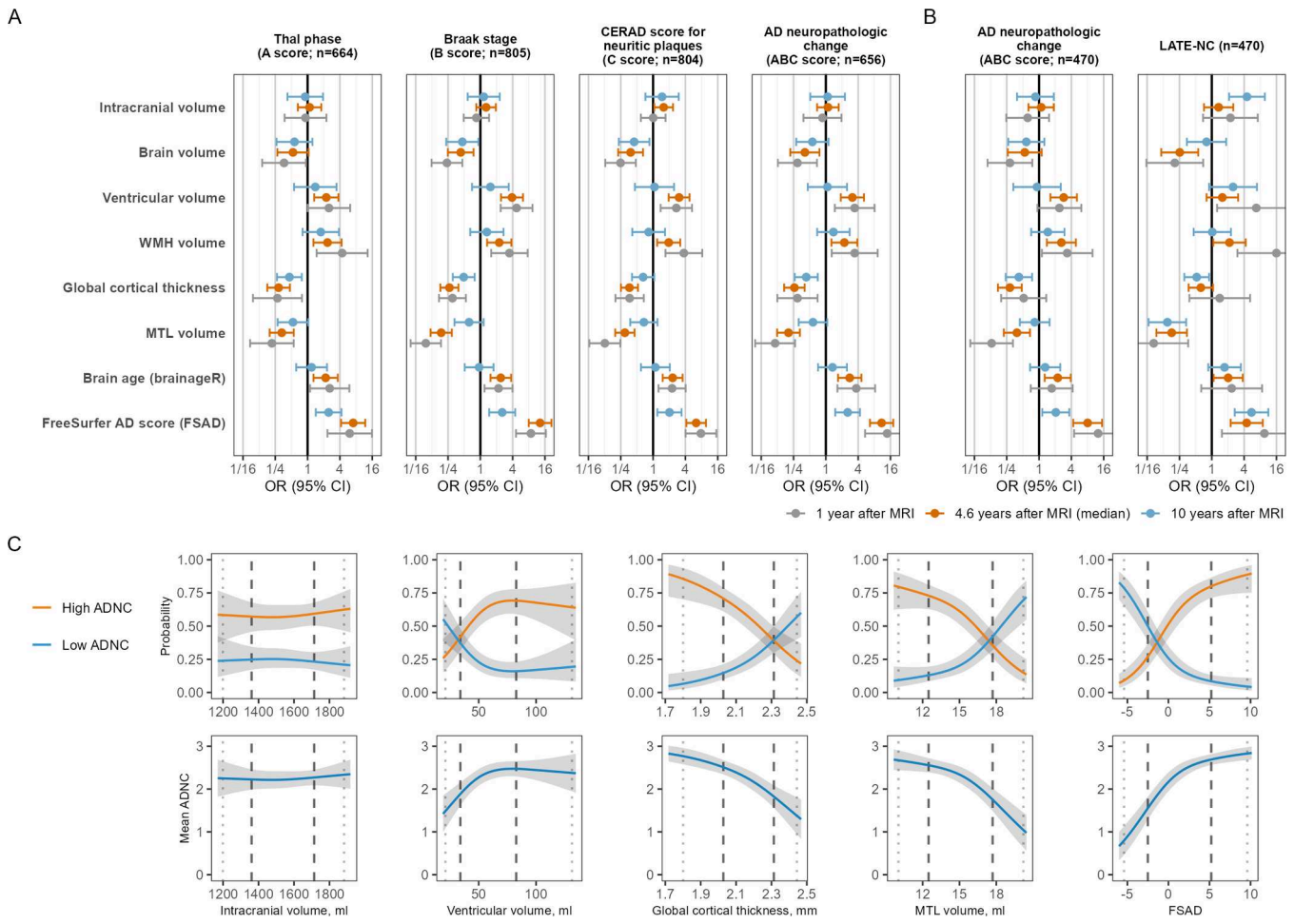

Fig. 2. Associations of MRI markers with AD neuropathology. (A) Odds ratios adjusted for age, sex, intracranial volume, study, magnetic field strength, and different time intervals between MRI and death (1 year, the median value of 4.6 years, and 10 years) (model 1). (**B**) Odds ratios estimated from the subsample with both data on ADNC and LATE-NC. (**C**) Probabilities of low and high AD neuropathologic change (ADNC) as well as mean ADNC for intracranial volume and the four most strongly associated MRI markers. Estimates are adjusted to a 78 year old male (intracranial volume=1,527 ml, participant at an ADRC, magnetic field strength=3T, time interval=4.6 years). ORs were defined by comparing the predicted odds at the 84 % quantile of exposure to the odds at the 16 % quantile (dashed lines). 2.5 % and 97.5 % quantiles indicated by dotted lines.

parameters.

3.2.5. *Primary structures of the medial temporal lobe*

Among the primary structures of the MTL, volume of the amygdala was most strongly associated with AD-related neuropathology.

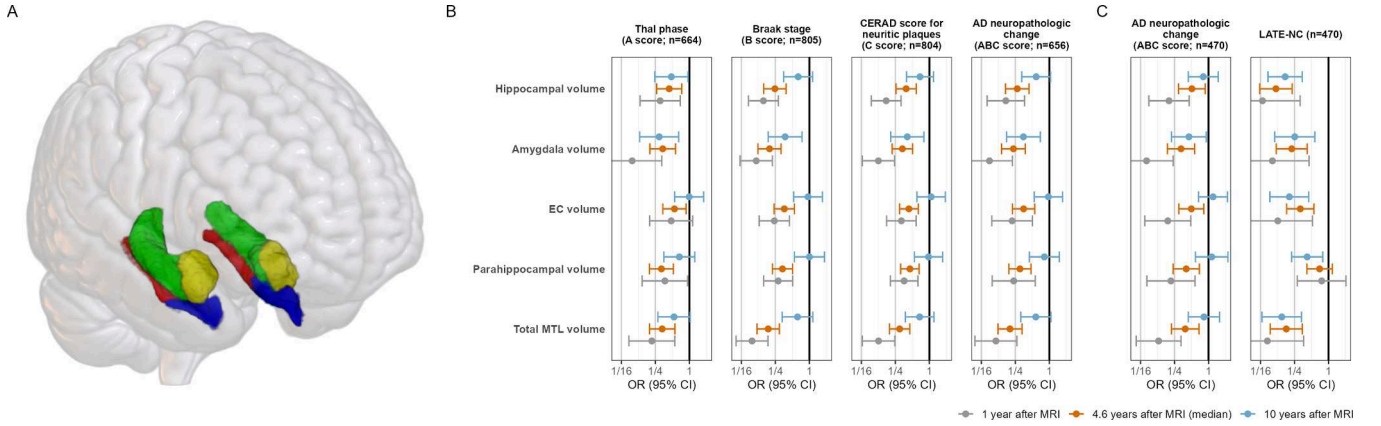

Fig. 3. Associations of primary structures of the medial temporal lobe with AD neuropathology. (A) The primary structures of the MTL are the hippocampus (green), the amygdala (yellow), the entorhinal cortex (blue), and the parahippocampal cortex (red). (**B**) Associations with AD neuropathology for different time intervals (1 year, the median value of 4.6 years, and 10 years) (model 1; *n*=659). (**C**) Odds ratios estimated from the subsample with both data on ADNC and LATE-NC. EC – entorhinal cortex.

However, confidence intervals were largely overlapping with those for other structures (Fig. 3B). Ten years after MRI, the amygdala was the only primary structure of the MTL whose volume was statistically significantly associated with ADNC at the 5 % level (OR=0.35, 95 % CI: 0.18-0.70). High hippocampal volume was associated with an OR of 0.58 (95 % CI: 0.32-1.05). In the subsample with available LATE-NC data, associations with LATE-NC were stronger than with ADNC for all regions except the parahippocampal cortex (Fig. 3C). The hippocampus showed the strongest association, with lower volume associated with 8.5-fold higher odds of LATE-NC compared to 2-fold higher odds of ADNC under model 1. Associations with LATE-NC remained similarly strong, whereas those with ADNC were attenuated, when adjusting for a time interval of 10 years between MRI and autopsy.

4. Discussion

In this study, data from 805 individuals from twenty ADRCs and the ADNI, who died between 2006 and 2024 and received T1-weighted brain MRI at least once before their death, were analyzed. MTL volume and the FSAD score were most strongly associated with AD neuropathology. In ordinal logistic regression models, low MTL volume was associated with 5-fold higher odds of ADNC, defined according current NIA-AA guidelines (Hyman et al., 2012, Montine et al., 2012). The odds ratio associated with a high FSAD score was 11. MTL volume and the FSAD score were also most strongly associated with ADNC after additional adjustment differences in cognitive status, with estimates of odds ratios being about half as large. This attenuation is consistent with the notion that both brain atrophy and neuropathology contribute to clinical symptoms. Conditioning on dementia status may attenuate the associations due to collider bias. For this reason, cognitive status was not included in the primary model (model 1). Taken together, these findings confirm the prominent role of the MTL as a target structure for structural imaging of AD. Volume of the MTL is one of the best validated AD markers and our results are consistent with previous clinico-pathological studies (Frisoni et al., 2017, Scheltens et al., 2021). There were no major differences in results from scans acquired at 1.5T compared to 3T. This was also the case when comparing results between the ADRCs and ADNI, although the comparably small sample size of the latter did not allow precise comparisons.

MRI markers correlated equally or more strongly with Braak stage (B score) than with Thal phase (A score) or density of neuritic plaques (C score), which has also been reported by past studies (Josephs et al., 2008, Vemuri et al., 2008, Dallaire-Théroux et al., 2019). This is in line with studies showing that cognitive decline in AD is more directly related to markers of tau than Aβ pathology (Bejanin et al., 2017, Huber et al., 2018). For instance, the estimated odds ratios associated with high a FSAD score was 6.3 for neuritic plaque burden (C score) but 13.0 for the Braak score (B score). Indeed, the spatial pattern of brain atrophy in AD mirrors the progression of NFT pathology (Whitwell et al., 2008), which was described by Braak and Braak more than 30 years ago (Braak and Braak, 1991). In the early stages, NFT pathology is confined to the MTL and only later spreads to large parts of the cortex, associated with cognitive and functional impairments. This might also explain the weaker association of MTL volume with ADNC in analyses restricted to individuals with dementia. While MTL volume appears to be excellent marker in the early phase of the disease, it seems rather insensitive to the neuropathological changes in the advanced phase of the disease. In contrast, markers capturing widespread atrophy of cerebral cortex such as global cortical thickness, brain age, or the FSAD score, were at least as strongly associated with ADNC in individuals with dementia as in those without in our study.

The number of subjects included in our study is large compared to previous ones (Dallaire-Théroux et al., 2017). It is therefore not surprising that, except for the intracranial volume that could be considered as a “control”, all MRI markers were statistically significantly associated with ADNC and its three subscores at the 5 % level. However, only MTL volume and the FSAD score explained substantial parts of the variation in ADNC in our sample (Nagelkerke’s $R^2 > 0.2$). The odds ratio of ADNC associated with a high FSAD score was 11 and the concordance index was 0.75, indicating a moderate overall discriminative accuracy. In binary logistic regression of high ADNC (versus intermediate/low/not AD), the associated odds ratios was 18.1 and the concordance index was 0.81. These odds ratios are much larger compared to those observed in many other studies of AD biomarkers. However, concordance indices between 0.7 and 0.8 are acceptable at best (de et al., 2022). Our study provides another example of the fact that large odds ratios are required for biomarkers to allow for meaningful predictions on the individual level and not only on the population-level (Pepe et al., 2004).

The strength of associations in our study are about equal or slightly larger than those reported in the few previous studies. For instance, Dallaire-Théroux et al. (Dallaire-Théroux et al., 2019) classified Braak stages of 186 subjects based 232 cortical and subcortical brain characteristics alongside of age, sex, time between MRI and death, and APOE4 status (Dallaire-Théroux et al., 2019). The mean time between MRI and death was 2.6 years and internally validated concordance indices for different dichotomizations ranged between 0.69 and 0.77. One interesting line of future research seems to be the integration of AD markers from other modalities, e.g. clinical factors (Carlson et al., 2015, Phongpreecha et al., 2023) or blood plasma markers (Bermudez et al., 2023), into joint prediction models of AD neuropathology. However, developing and validating prediction models of AD neuropathology was not the main focus of our study and requires the investigation of additional aspects of prediction quality, e.g. calibration performance (Van Calster et al., 2019).

Our study also included an estimate of brain age (brainageR), which was statistically significantly associated with ADNC and all three subscores at the 5 % level. In a recent analyses of 1,140 patients of a memory clinic in the UK, patients with higher values of brainageR compared to their chronological age were at higher risk of developing dementia with an estimated hazard ratio of 1.03 per one year difference (Biondo et al., 2022). The concept of structural brain age is attractive, as it only requires a single MRI scan and the chronological age of the patient. Advanced brain ageing has been found to be correlated with AD biomarkers such amyloid-positivity on positron emission tomography and cerebrospinal fluid levels of Aβ and phosphorylated tau (Cumplido-Mayoral et al., 2023). However, the associated odds ratios in our study were much smaller than those for MTL volume or the FSAD score. Although brainageR seems to be an excellent method for assessing the biological age of the brain, it did not capture the neuropathology of AD better than apparently simpler markers such as ventricular volume or global cortical thickness in our study. Ratings of neuropathology correlated with a spatial pattern of brain atrophy that was most pronounced in the MTL and differed from that of “normal” ageing. This is line with AD being a distinct brain disorder and not a “advanced” or “accelerated” form of normal ageing, as pointed out by pathologist for quite some time (Nelson et al., 2011).

Our main analyses included an interaction with time between MRI and death and were adjusted for the sample median of 4.9 years. Odds ratios from analyses adjusted for longer time intervals were much smaller. For instance, the odds ratio of ADNC associated with a high FSAD score one year after MRI was 13.9 (95 % CI: 5.4-35.8), but was only 2.5 (95 % CI: 1.5-4.3) ten years after. There may be two reasons for this. First, the predictive value of MRI markers may decline with time because of additional factors influencing the progression of AD neuropathology after the time of MRI. Second, highly abnormal values of structural MRI markers in individuals who survived for ten or more years are more likely false positives, i.e. they are less likely to actually have dementia. Studies in US cohorts found that people with age 65 or older only survive an average four to eight years after initial diagnosis of AD (2024). Odds ratios adjusted for long time intervals should therefore be interpreted with caution.

Analyses of the primary structure of the MTL suggest differential

associations with AD neuropathology. Amygdala volume was most strongly associated with ADNC, followed by hippocampal volume, albeit confidence intervals were largely overlapping. Indeed, early studies highlighted the amygdala as an early site of AD neuropathology (Vogt et al., 1990, Stouffer et al., 2024). Ten years after MRI, only amygdala volume was statistically significantly associated with ADNC at the 5 % level. Brain atrophy in AD is thus best assessed by an aggregate index that weighs individual brain regions and such an index should be preferred over volumetric characteristics of single brain regions. Several methodological approaches for deriving such an index, including the FSAD score in the present study, have been successfully applied in the past (Frenzel et al., 2020, Thompson et al., 2003, Teipel et al., 2007, Vemuri et al., 2008, Lerch et al., 2008, Klöppel et al., 2008, Duchesne et al., 2008, Davatzikos et al., 2009, Moradi et al., 2015, Beheshti and Demirel, 2016, Lee et al., 2019). However, systematic validation against AD neuropathology and comparisons to "simpler" markers have been lacking so far. Both in the total sample and in subsamples of individuals without and with dementia, the FSAD score was at least as strongly associated with the neuropathology of AD as other commonly used markers, e.g. hippocampal volume.

Our study included all participants in ADRCs and ADNI who underwent autopsy and had at least one MRI scan prior to death. It was not restricted to cases of pure AD neuropathology. Co-pathologies likely contributed to the structural changes observed in these participants, with LATE-NC being particularly relevant, as it frequently co-occurs with AD and is also associated with MTL atrophy (Josephs et al., 2017, Yu et al., 2020, Teipel and Grothe, 2023). Analyses in the subset of study participants with available data on LATE-NC showed a weak positive association with ADNC, i.e. subjects with high ADNC were slightly more likely to also have LATE-NC at autopsy. Importantly, the estimated odds ratios of ADNC associated with the MRI markers were practically unchanged when additionally adjusting for LATE-NC in the regression models. At the same time, MTL atrophy was as strongly associated with LATE-NC as with ADNC. Hippocampal atrophy was mainly associated with LATE-NC at autopsy, consistent with previous studies (Josephs et al., 2008, Josephs et al., 2017, Yu et al., 2020, Teipel and Grothe, 2023), whereas the FSAD score showed stronger associations with ADNC than with LATE-NC. These findings suggest that LATE-NC and ADNC independently and additively contributed to MTL atrophy in our sample. With respect to LATE-NC, analyses of MTL substructures showed heterogeneity, with weak associations for the parahippocampal gyrus and stronger associations for other MTL regions, particularly the hippocampus, across all examined time intervals. These results are in line with previous studies reporting more pronounced hypometabolism and atrophy of the inferior temporal lobe (Teipel and Grothe, 2023, Grothe et al., 2023, Botha et al., 2018, Buciuc et al., 2020). The ratio of parahippocampal gyrus volume to anterior hippocampus volume has been suggested as marker of TDP-43 pathology (de Flores et al., 2020). Taken together, our results support that patterns of atrophy within the MTL may serve as markers for LATE-NC, warranting further investigation.

Our study has several limitations. ADNI and the ADRCs recruit subject at multiple sites in the US and Canada but we did not consider population differences between these sites, e.g. with respect to ethnicity. Our results may therefor not generalize to other populations. There also was considerably variation in the time between MRI and autopsy with values up to 16 years. For estimating associations with MRI markers, autopsies should ideally be performed shortly after the time of MRI, however. To address this, regression models included an interaction of the respective MRI marker with length of the time interval, instead of excluding subjects with longer intervals exceeding a subjectively chosen threshold. While ADRCs all follow the same procedures for neuropathologic examinations, they are performed by different laboratories which may induce additional variation. In addition, there was considerably heterogeneity with respect to MRI acquisition parameters. Scans from ADRCs were acquired with varying protocols and parameters. Scans were acquired both at 1.5T and 3T, which may bias estimates of morphometric brain characteristics. For instance, estimates of cortical thickness tend to be larger at 3T (Han et al., 2006). However, there were no major differences in results from scans acquired at 1.5T versus 3T in our study, and, in addition, main analyses were adjusted for differences in magnetic field strength. Furthermore, semi-quantitative neuropathology ratings are subject to ceiling effects and have limited dynamic range compared with quantitative measures such as regional tangle counts (Denning et al., 2024). Finally, except brain age, all MRI markers were determined with the image-processing suite FreeSurfer, and results derived using other processing software may differ.

A major strength of our study is its reliance on two large repositories of neuropathology data that were collected in a highly standardized manner. Associations were investigated using ordinal logistic regression models, which do not make any assumption on the distributions of the semi-quantitative ratings. Previous studies mostly relied on binary logistic regressions, which requires selecting an arbitrary threshold value. Importantly, the confidence interval obtained from the ordinal regression models were much narrower than those from binary logistic models. On the log-odds scale, the standard error of the effect estimate for the association between ADNC on the FSAD in model 1 is only 62 % of the standard error from the binary model based on a threshold value of 3 (high vs. intermediate/low/no ADNC). To achieve the same precision, the binary model would thus require a sample size of 1,062 instead of the 656 available in our study. When ADNC is dichotomized at a threshold of 1 (high/intermediate/low vs. no ADNC), the efficiency of the binary model is even lower (37 %) and it would even require 1,771 cases to achieve the same precision as the ordinal model. We also carefully considered the role of image quality parameter as potential unwanted mediators of associations of AD neuropathology with MRI markers. Notably, the signal-to-noise ratio in gray matter was as strongly associated with ADNC as total brain volume, ventricular volume, and volume of white matter hypointensities, presumably due to more frequent head movements in individuals with cognitive impairments (Hausman et al., 2022). While the results in our study were robust against differences in image quality, it seems that one must proceed with caution when developing markers that directly assess signal intensities or texture features from MRI scans.

In summary, AD neuropathology ratings according current NIA-AA guidelines were associated with a distinct pattern of atrophy most pronounced in, but not restricted to, the MTL. The present study extends previous ones, which relied on smaller samples and often considered only specific aspects of AD neuropathology (Dallaire-Théroux et al., 2017). It confirms the importance of the MTL as a target for structural imaging in AD (Frisoni et al., 2017, Scheltens et al., 2021). An aggregate index of AD-related brain atrophy that is also sensitive to atrophy outside the MTL in the advanced phase of the disease, was most strongly associated with AD neuropathology. Several such indices were suggested in the past but they still appear to be niche and are not widely used in clinical research. Our results provide further evidence to prefer such indices over morphometric characteristics of single brain regions (e.g. hippocampal volume) for enriching samples or as secondary outcomes in clinical trials of AD.

Funding

The NACC database is funded by NIA/NIH Grant U24 AG072122. NACC data are contributed by the NIA-funded ADRCs: P30 AG062429 (PI James Brewer, MD, PhD), P30 AG066468 (PI Oscar Lopez, MD), P30 AG062421 (PI Bradley Hyman, MD, PhD), P30 AG066509 (PI Thomas Grabowski, MD), P30 AG066514 (PI Mary Sano, PhD), P30 AG066530 (PI Helena Chui, MD), P30 AG066507 (PI Marilyn Albert, PhD), P30 AG066444 (PI David Holtzman, MD), P30 AG066518 (PI Lisa Silbert, MD, MCR), P30 AG066512 (PI Thomas Wisniewski, MD), P30 AG066462 (PI Scott Small, MD), P30 AG072979 (PI David Wolk, MD), P30 AG072972 (PI Charles DeCarli, MD), P30 AG072976 (PI Andrew

Saykin, PsyD), P30 AG072975 (PI Julie A. Schneider, MD, MS), P30 AG072978 (PI Ann McKee, MD), P30 AG072977 (PI Robert Vassar, PhD), P30 AG066519 (PI Frank LaFerla, PhD), P30 AG062677 (PI Ronald Petersen, MD, PhD), P30 AG079280 (PI Jessica Langbaum, PhD), P30 AG062422 (PI Gil Rabinovici, MD), P30 AG066511 (PI Allan Levey, MD, PhD), P30 AG072946 (PI Linda Van Eldik, PhD), P30 AG062715 (PI Sanjay Asthana, MD, FRCP), P30 AG072973 (PI Russell Swerdlow, MD), P30 AG066506 (PI Glenn Smith, PhD, ABPP), P30 AG066508 (PI Stephen Strittmatter, MD, PhD), P30 AG066515 (PI Victor Henderson, MD, MS), P30 AG072947 (PI Suzanne Craft, PhD), P30 AG072931 (PI Henry Paulson, MD, PhD), P30 AG066546 (PI Sudha Seshadri, MD), P30 AG086401 (PI Erik Roberson, MD, PhD), P30 AG086404 (PI Gary Rosenberg, MD), P20 AG068082 (PI Angela Jefferson, PhD), P30 AG072958 (PI Heather Whitson, MD), P30 AG072959 (PI James Leverenz, MD).

Data collection and sharing for this project was funded by the Alzheimer's Disease Neuroimaging Initiative (ADNI) (National Institutes of Health Grant U01 AG024904) and DOD ADNI (Department of Defense award number W81XWH-12-2-0012). ADNI is funded by the National Institute on Aging, the National Institute of Biomedical Imaging and Bioengineering, and through generous contributions from the following: AbbVie, Alzheimer's Association; Alzheimer's Drug Discovery Foundation; Araclon Biotech; BioClinica, Inc.; Biogen; Bristol-Myers Squibb Company; CereSpir, Inc.; Cogstate; Eisai Inc.; Elan Pharmaceuticals, Inc.; Eli Lilly and Company; EuroImmun; F. Hoffmann-La Roche Ltd and its affiliated company Genentech, Inc.; Fujirebio; GE Healthcare; IXICO Ltd.; Janssen Alzheimer Immunotherapy Research & Development, LLC.; Johnson & Johnson Pharmaceutical Research & Development LLC.; Lumosity; Lundbeck; Merck & Co., Inc.; Meso Scale Diagnostics, LLC.; NeuroRx Research; Neurotrack Technologies; Novartis Pharmaceuticals Corporation; Pfizer Inc.; Piramal Imaging; Servier; Takeda Pharmaceutical Company; and Transition Therapeutics. The Canadian Institutes of Health Research is providing funds to support ADNI clinical sites in Canada. Private sector contributions are facilitated by the Foundation for the National Institutes of Health (www.fnih.org). The grantee organization is the Northern California Institute for Research and Education, and the study is coordinated by the Alzheimer's Therapeutic Research Institute at the University of Southern California. ADNI data are disseminated by the Laboratory for Neuro Imaging at the University of Southern California.

This study was further supported by the Federal Ministry of Education and Research Germany (project PoSyMed: Population Systems Medicine for De Novo Mechanotyping of Complex Diseases; 031L0310B).

Ethics statement

Research using the NACC database was approved by the University of Washington Institutional Review Board and informed consent was obtained from all participants and/or authorized representatives at the individual ADRCs. Data collection and sharing in ADNI was approved by the Institutional Review Board of each participating institution. Written informed consent was obtained from all ADNI participants and/or authorized representatives before any protocol-specific procedures were carried out. All procedures involving human participants were in accordance with the ethical standards of the 1964 Helsinki Declaration and its later amendments.

Data and code availability statement

Data of the NACC and the ADNI are accessible after registration. For more information we refer to www.naccdata.org and adni.loni.usc.edu. MRI markers considered in this study were derived using the Freesurfer image analysis suite, which is documented and freely available for download online (http://surfer.nmr.mgh.harvard.edu). The parameters required for deriving the FSAD score from the output of FreeSurfer are provided by Supplementary Table 1. Brain age scores were derived using the brainageR software (version 2.1; https://github.com/james-cole/brainageR). Statistical analyses were performed with the *rms* package in *R*. Code for model fitting, odds ratio estimation, and generation of prediction plots is provided as supplementary material.

CRediT authorship contribution statement

Stefan Frenzel: Writing – original draft, Formal analysis, Data curation, Conceptualization. **Stefan J. Teipel:** Writing – review & editing, Conceptualization. **Hans J. Grabe:** Writing – review & editing, Conceptualization.

Declaration of competing interest

H.J.G. has received travel grants and speaker honoraria from Indorsia, Neuraxpharm, Servier, and Janssen Cilag. H.J.G. had personal contracts approved by the university administration for speaker honoraria. S.F. and S.J.T. have nothing to disclose.

Supplementary materials

Supplementary material associated with this article can be found, in the online version, at doi:10.1016/j.neuroimage.2026.121841.

References

2024 Alzheimer's disease facts and figures. Alzheimers. Dement. 20, 2024, 3708–3821.
Beekly, D.L., Ramos, E.M., van Belle, G., Deitrich, W., et al., 2004. The National Alzheimer's Coordinating Center (NACC) Database: an Alzheimer disease database. Alzheimer Dis. Assoc. Disord. 18, 270–277.
Beekly, D.L., Ramos, E.M., Lee, W.W., Deitrich, W.D., et al., 2007. The National Alzheimer's Coordinating Center (NACC) database: the Uniform Data Set. Alzheimer Dis. Assoc. Disord. 21, 249–258.
Beheshti, I., Demirel, H., 2016. Feature-ranking-based Alzheimer's disease classification from structural MRI. Magn. Reson. ImAging 34, 252–263.
Bejanin, A., Schonhaut, D.R., La Joie, R., Kramer, J.H., et al., 2017. Tau pathology and neurodegeneration contribute to cognitive impairment in Alzheimer's disease. Brain 140, 3286–3300.
Bennett, D.A., Schneider, J.A., Arvanitakis, Z., Kelly, J.F., et al., 2006. Neuropathology of older persons without cognitive impairment from two community-based studies. Neurology 66, 1837–1844.
Bermudez, C., Graff-Radford, J., Syrjanen, J.A., Stricker, N.H., et al., 2023. Plasma biomarkers for prediction of Alzheimer's disease neuropathologic change. Acta Neuropathol. 146, 13–29.
Besser, L., Kukull, W., Knopman, D.S., Chui, H., et al., 2018. Version 3 of the National Alzheimer's Coordinating Center's Uniform Data Set. Alzheimer Dis. Assoc. Disord. 32, 351–358.
Besser, L.M., Kukull, W.A., Teylan, M.A., Bigio, E.H., et al., 2018. The Revised National Alzheimer's Coordinating Center's neuropathology form-available data and new analyses. J. Neuropathol. Exp. Neurol. 77, 717–726.
Biondo, F., Jewell, A., Pritchard, M., Aarsland, D., et al., 2022. Brain-age is associated with progression to dementia in memory clinic patients. NeuroImage: Clin. 36, 103175.
Botha, H., Mantyh, W.G., Murray, M.E., Knopman, D.S., et al., 2018. FDG-PET in tau-negative amnestic dementia resembles that of autopsy-proven hippocampal sclerosis. Brain 141, 1201–1217.
Boyle, P.A., Yu, L., Wilson, R.S., Leurgans, S.E., et al., 2018. Person-specific contribution of neuropathologies to cognitive loss in old age. Ann. Neurol. 83, 74–83.
Braak, H., Braak, E., 1991. Neuropathological stageing of Alzheimer-related changes. Acta Neuropathol. 82, 239–259.
Buciuc, M., Botha, H., Murray, M.E., Schwarz, C.G., et al., 2020. Utility of FDG-PET in diagnosis of Alzheimer-related TDP-43 proteinopathy. Neurology 95, e23–e34.
Carlson, J.O.E., Gatz, M., Pedersen, N.L., Graff, C., et al., 2015. Antemortem prediction of Braak stage. J. Neuropathol. Exp. Neurol. 74, 1061–1070.
Cole, J.H., Ritchie, S.J., Bastin, M.E., Hernández, M.C.V., et al., 2018. Brain age predicts mortality. Mol. Psychiatry 23, 1385–1392.
Consensus recommendations for the postmortem diagnosis of Alzheimer's disease. The National Institute on Aging, and Reagan Institute Working Group on Diagnostic Criteria for the Neuropathological Assessment of Alzheimer's Disease. Neurobiol. Aging 18, 1997, S1–S2.
Cumplido-Mayoral, I., García-Prat, M., Operto, G., Falcon, C., et al., 2023. Biological brain age prediction using machine learning on structural neuroimaging data: multi-cohort validation against biomarkers of Alzheimer's disease and neurodegeneration stratified by sex. Elife 12, e81067.
Dallaire-Théroux, C., Callahan, B.L., Potvin, O., Saikali, S., et al., 2017. Radiological-pathological correlation in Alzheimer's Disease: systematic review of antemortem Magnetic resonance imaging findings. J. Alzheimers. Dis. 57, 575–601.

Dallaire-Théroux, C., Beheshti, I., Potvin, O., Dieumegarde, L., et al., 2019. Braak neurofibrillary tangle staging prediction from in vivo MRI metrics. Alzheimers. Dement. 11, 599–609.
Davatzikos, C., Xu, F., An, Y., Fan, Y., et al., 2009. Longitudinal progression of Alzheimer's-like patterns of atrophy in normal older adults: the SPARE-AD index. Brain 132, 2026–2035.
de Flores, R., Wisse, L.E.M., Das, S.R., Xie, L., et al., 2020. Contribution of mixed pathology to medial temporal lobe atrophy in Alzheimer's disease. Alzheimers. Dement. 16, 843–852.
Denning, A.E., Ittyerah, R., Levorse, L.M., Sadeghpour, N., et al., 2024. Association of quantitative histopathology measurements with antemortem medial temporal lobe cortical thickness in the Alzheimer's disease continuum. Acta Neuropathol. 148, 37.
Desikan, R.S., Ségonne, F., Fischl, B., Quinn, B.T., et al., 2006. An automated labeling system for subdividing the human cerebral cortex on MRI scans into gyral based regions of interest. Neuroimage 31, 968–980.
Duchesne, S., Caroli, A., Geroldi, C., Barillot, C., et al., 2008. MRI-based automated computer classification of probable AD versus normal controls. IEEe Trans. Med. ImAging 27, 509–520.
Enkirch, S.J., Traschütz, A., Müller, A., Widmann, C.N., et al., 2018. The ERICA Score: an MR imaging-based visual scoring system for the assessment of entorhinal cortex atrophy in Alzheimer Disease. Radiology 288, 226–333.
Esteban, O., Birman, D., Schaer, M., Koyejo, O.O., et al., 2017. MRIQC: advancing the automatic prediction of image quality in MRI from unseen sites. PLoS. One 12, e0184661.
Fischl, B., 2012. FreeSurfer. Neuroimage 62, 774–781.
Franke, K., Gaser, C., 2019. Ten years of BrainAGE as a neuroimaging biomarker of brain aging: what insights have we gained? Front. Neurol. 10, 789.
Frenzel, S., Wittfeld, K., Habes, M., Klinger-König, J., et al., 2020. A biomarker for Alzheimer's disease based on patterns of regional brain atrophy. Front. Psychiatry 10, 953.
Frisoni, G.B., Fox, N.C., Jack, Jr.CR, Scheltens, P., et al., 2010. The clinical use of structural MRI in Alzheimer disease. Nat. Rev. Neurol. 6, 67–77.
Frisoni, G.B., Boccardi, M., Barkhof, F., Blennow, K., et al., 2017. Strategic roadmap for an early diagnosis of Alzheimer's disease based on biomarkers. Lancet Neurol. 16, 661–676.
Gelman, A., 2008. Scaling regression inputs by dividing by two standard deviations. Stat. Med. 27, 2865–2873.
Grothe, M.J., Moscoso, A., Silva-Rodríguez, J., Lange, C., et al., 2023. Differential diagnosis of amnestic dementia patients based on an FDG-PET signature of autopsy-confirmed LATE-NC. Alzheimers. Dement. 19, 1234–1244.
Haller, S., Jäger, H.R., Vernooij, M.W., Barkhof, F., 2023. Neuroimaging in dementia: more than typical Alzheimer disease. Radiology 308, e230173.
Han, X., Jovicich, J., Salat, D., van der Kouwe, A., et al., 2006. Reliability of MRI-derived measurements of human cerebral cortical thickness: the effects of field strength, scanner upgrade and manufacturer. Neuroimage 32, 180–194.
Harrell, F., 2015. Regression Modeling Strategies: With Applications to Linear Models, Logistic and Ordinal Regression, and Survival Analysis. Springer International Publishing.
Hausman, H.K., Hardcastle, C., Kraft, J.N., Evangelista, N.D., et al., 2022. The association between head motion during functional magnetic resonance imaging and executive functioning in older adults. Neuroimage: Rep. 2, 100085.
Hond AAH, de, EW, Steyerberg, van, Calster B, 2022. Interpreting area under the receiver operating characteristic curve. Lancet Digit. Health 4, e853–e855.
Huber, C.M., Yee, C., May, T., Dhanala, A., et al., 2018. Cognitive decline in preclinical Alzheimer's disease: amyloid-beta versus tauopathy. J. Alzheimers. Dis. 61, 265–281.
Hyman, B.T., Phelps, C.H., Beach, T.G., Bigio, E.H., et al., 2012. National Institute on Aging–Alzheimer's Association guidelines for the neuropathologic assessment of Alzheimer's disease. Alzheimer's Dement. 8, 1–13.
Jack, C.R., Holtzman, D.M., 2013. Biomarker modeling of Alzheimer's disease. Neuron 80, 1347–1358.
Jack, C.R., Knopman, D.S., Jagust, W.J., Petersen, R.C., et al., 2013. Tracking pathophysiological processes in Alzheimer's disease: an updated hypothetical model of dynamic biomarkers. Lancet Neurol. 12, 207–216.
Jack, Jr.CR, DA, Bennett, K, Blennow, MC, Carrillo, et al., 2018. NIA-AA Research Framework: toward a biological definition of Alzheimer's disease. Alzheimer's Dement. 14, 535–562.
Jack Jr, C.R., A, Arani, BJ, Borowski, DM, Cash, et al., 2024. Overview of ADNI MRI. Alzheimer's Dement. 20, 7350–7360.
Josephs, K.A., Whitwell, J.L., Knopman, D.S., Hu, W.T., et al., 2008. Abnormal TDP-43 immunoreactivity in AD modifies clinicopathologic and radiologic phenotype. Neurology 70, 1850–1857.
Josephs, K.A., Whitwell, J.L., Ahmed, Z., Shiung, M.M., et al., 2008. Beta-amyloid burden is not associated with rates of brain atrophy. Ann. Neurol. 63, 204–212.
Josephs, K.A., Murray, M.E., Whitwell, J.L., Parisi, J.E., et al., 2014. Staging TDP-43 pathology in Alzheimer's disease. Acta Neuropathol. 127, 441–450.
Josephs, K.A., Dickson, D.W., Tosakulwong, N., Weigand, S.D., et al., 2017. Rates of hippocampal atrophy and presence of post-mortem TDP-43 in patients with Alzheimer's disease: a longitudinal retrospective study. Lancet Neurol. 16, 917–924.
Katsumata, Y., Abner, E.L., Karanth, S., Teylan, M.A., et al., 2020. Distinct clinicopathologic clusters of persons with TDP-43 proteinopathy. Acta Neuropathol. 140, 659–674.
Klöppel, S., Stonnington, C.M., Chu, C., Draganski, B., et al., 2008. Automatic classification of MR scans in Alzheimer's disease. Brain 131, 681–689.
Lee, E., Choi, J-S, Kim, M., Suk, H-I, 2019. Toward an interpretable Alzheimer's disease diagnostic model with regional abnormality representation via deep learning. Neuroimage 202, 116113.
Leocadi, M., Canu, E., Calderaro, D., Corbetta, D., et al., 2020. An update on magnetic resonance imaging markers in AD. Ther. Adv. Neurol. Disord. 13.
Lerch, J.P., Pruessner, J., Zijdenbos, A.P., Collins, D.L., et al., 2008. Automated cortical thickness measurements from MRI can accurately separate Alzheimer's patients from normal elderly controls. Neurobiol. Aging 29, 23–30.
Mirra, S.S., Hart, M.N., Terry, R.D., 1993. Making the diagnosis of Alzheimer's disease. A primer for practicing pathologists. Arch. Pathol. Lab. Med. 117, 132–144.
Montine, T.J., Phelps, C.H., Beach, T.G., Bigio, E.H., et al., 2012. National Institute on Aging-Alzheimer's Association guidelines for the neuropathologic assessment of Alzheimer's disease: a practical approach. Acta Neuropathol. 123, 1–11.
Moradi, E., Pepe, A., Gaser, C., Huttunen, H., et al., 2015. Machine learning framework for early MRI-based Alzheimer's conversion prediction in MCI subjects. Neuroimage 104, 398–412.
Mueller, S.G., Weiner, M.W., Thal, L.J., Petersen, R.C., et al., 2005. The Alzheimer's Disease Neuroimaging Initiative. NeuroimAging Clin. N. Am. 15, 869–xii.
Nagelkerke, N.J., 1991. A note on a general definition of the coefficient of determination. Biometrika 78, 691–692.
Nelson, P.T., Head, E., Schmitt, F.A., Davis, P.R., et al., 2011. Alzheimer's disease is not "brain aging": neuropathological, genetic, and epidemiological human studies. Acta Neuropathol. 121, 571–587.
Nelson, P.T., Dickson, D.W., Trojanowski, J.Q., Jack, C.R., et al., 2019. Limbic-predominant age-related TDP-43 encephalopathy (LATE): consensus working group report. Brain 142, 1503–1527.
Pepe, M.S., Janes, H., Longton, G., Leisenring, W., et al., 2004. Limitations of the odds ratio in gauging the performance of a diagnostic, prognostic, or screening marker. Am. J. Epidemiol. 159, 882–890.
Perrin, R.J., Franklin, E.E., Bernhardt, H., Burns, A., et al., 2024. The Alzheimer's Disease Neuroimaging Initiative Neuropathology Core: an update. Alzheimers. Dement. 20, 7859–7870.
Phongpreecha, T., Cholerton, B., Bukhari, S., Chang, A.L., et al., 2023. Prediction of neuropathologic lesions from clinical data. Alzheimers. Dement. 19, 3005–3018.
Pini, L., Pievani, M., Bocchetta, M., Altomare, D., et al., 2016. Brain atrophy in Alzheimer's Disease and aging. Ageing Res. Rev. 30, 25–48.
Reuter, M., Tisdall, M.D., Qureshi, A., Buckner, R.L., et al., 2015. Head motion during MRI acquisition reduces gray matter volume and thickness estimates. Neuroimage 107, 107–115.
Robinson, J.L., Lee, E.B., Xie, S.X., Rennert, L., et al., 2018. Neurodegenerative disease concomitant proteinopathies are prevalent, age-related and APOE4-associated. Brain 141, 2181–2193.
Rorden, C., 2025. MRIcroGL: voxel-based visualization for neuroimaging. Nat. Methods 22, 1613–1614.
Scheltens, P., Leys, D., Barkhof, F., Huglo, D., et al., 1992. Atrophy of medial temporal lobes on MRI in "probable" Alzheimer's disease and normal ageing: diagnostic value and neuropsychological correlates. J. Neurol. Neurosurg. Psychiatry 55, 967–972.
Scheltens, P., De Strooper, B., Kivipelto, M., Holstege, H., et al., 2021. Alzheimer's disease. Lancet 397, 1577–1590.
Schwahn, C., Frenzel, S., Holtfreter, B., Van der Auwera, S., et al., 2022. Effect of periodontal treatment on preclinical Alzheimer's disease - results of a trial emulation approach. Alzheimer's Dement 18, 127–141.
Stouffer, K.M., Grande, X., Düzel, E., Johansson, M., et al., 2024. Amidst an amygdala renaissance in Alzheimer's disease. Brain 147, 816–829.
Teipel, S., Grothe, M.J., 2023. MRI-based basal forebrain atrophy and volumetric signatures associated with limbic TDP-43 compared to Alzheimer's disease pathology. Neurobiol. Dis. 180, 106070.
Teipel, S.J., Pruessner, J.C., Faltraco, F., Born, C., et al., 2006. Comprehensive dissection of the medial temporal lobe in AD: measurement of hippocampus, amygdala, entorhinal, perirhinal and parahippocampal cortices using MRI. J. Neurol. 253, 794–800.
Teipel, S.J., Born, C., Ewers, M., Bokde, A.L.W., et al., 2007. Multivariate deformation-based analysis of brain atrophy to predict Alzheimer's disease in mild cognitive impairment. Neuroimage 38, 13–24.
Thaker, A.A., Weinberg, B.D., Dillon, W.P., Hess, C.P., et al., 2017. Entorhinal cortex: antemortem cortical thickness and postmortem neurofibrillary tangles and amyloid pathology. AJNR Am. J. Neuroradiol. 38, 961–965.
Thal, D.R., Rüb, U., Orantes, M., Braak, H., 2002. Phases of A beta-deposition in the human brain and its relevance for the development of AD. Neurology. 58, 1791–1800.
Thompson, P.M., Hayashi, K.M., de, Zubicaray G, Janke, A.L., et al., 2003. Dynamics of gray matter loss in Alzheimer's disease. J. Neurosci. 23, 994–1005.
Van Calster, B., McLernon, D.J., van Smeden, M., Wynants, L., et al., 2019. Calibration: the Achilles heel of predictive analytics. BMC. Med. 17, 230.
Vemuri, P., Whitwell, J.L., Kantarci, K., Josephs, K.A., et al., 2008. Antemortem MRI based STructural Abnormality iNDex (STAND)-scores correlate with postmortem Braak neurofibrillary tangle stage. Neuroimage 42, 559–567.
Vemuri, P., Gunter, J.L., Senjem, M.L., Whitwell, J.L., et al., 2008. Alzheimer's disease diagnosis in individual subjects using structural MR images: validation studies. Neuroimage 39, 1186–1197.
Vogt, L.J.K., Hyman, B.T., Van Hoesen, G.W., Damasio, A.R., 1990. Pathological alterations in the amygdala in Alzheimer's disease. Neuroscience 37, 377–385.
Walker, S.H., Duncan, D.B., 1967. Estimation of the probability of an event as a function of several independent variables. Biometrika 54, 167–179.

Wei, K., Tran, T., Chu, K., Borzage, M.T., et al., 2019. White matter hypointensities and hyperintensities have equivalent correlations with age and CSF β-amyloid in the nondemented elderly. Brain Behav. 9, e01457.
Weiner, M.W., Veitch, D.P., Aisen, P.S., Beckett, L.A., et al., 2017. Recent publications from the Alzheimer's Disease Neuroimaging Initiative: reviewing progress toward improved AD clinical trials. Alzheimer's Dement. 13, e1–e85.
Whitwell, J.L., Josephs, K.A., Murray, M.E., Kantarci, K., et al., 2008. MRI correlates of neurofibrillary tangle pathology at autopsy: a voxel-based morphometry study. Neurology. 71, 743–749.
Wolk, D.A., Nelson, P.T., Apostolova, L., Arfanakis, K., et al., 2025. Clinical criteria for limbic-predominant age-related TDP-43 encephalopathy. Alzheimer's Dement. 21, e14202.
Woodworth, D.C., Nguyen, K.M., Sordo, L., Scambray, K.A., et al., 2024. Evaluating the updated LATE-NC staging criteria using data from NACC. Alzheimer's Dement. 20, 8359–8373.
Yu, L., Boyle, P.A., Dawe, R.J., Bennett, D.A., et al., 2020. Contribution of TDP and hippocampal sclerosis to hippocampal volume loss in older-old persons. Neurology 94, e142–e152.